RSC Advances

ROYAL SOCIETY OF CHEMISTRY

www.rsc.org/advances

RSC Advances

RSCPublishing

COMMUNICATION

Novel wood-based all-solid-state flexible supercapacitors fabricated with natural porous wood slice and polypyrrole

Cite this: DOI: 10.1039/xoxxoooooox

Shaoyi Lv,[a*] Feng Fu,[a] Siqun Wang,[a,b] Jingda Huang [a] and La Hu[a]

Received ooth January 2014,
Accepted ooth January 2014

DOI: 10.1039/xoxxoooooox

www.rsc.org/

We utilized a simple dipping-and-polymerization method to prepare an interesting electrode material consisting of polypyrrole (PPy) polymerized on wood transverse section slice (WTSS), and fabricated a wood-based supercapacitor. The novel electrode has a 3D honeycomb porous framework, a high capacitance (0.61 F cm^{-2}) and excellent flexibility. These make the PPy-coated WTSS electrode an excellent alternative candidate for flexible energy storage.

Introduction

Flexible supercapacitors show a considerable potential for applications in future flexible electronics due to their flexible, low cost, light-weight and environmental-friendly advantages.[1,2] The realization of highly flexible devices strongly depends on the mechanical flexibility of the electrode materials.[3,4] One simple way to create flexible electrode materials is to add active materials to a flexible substrate such as paper[5,6] and textile,[7,8] in order to form the composite electrode materials. These flexible substrates also have an excellent microscopic porous structure and hydrophilic characteristics that have a positive effect on the electrochemical performance of energy storage device.[9,10] The microporous characteristics of the substrates can provide large surface areas for electrochemical reaction of the active materials and shorten diffusion paths for the electrolyte ions on the one hand.[11] On the other hand, the hydrophilic properties of the substrates can absorb more electrolytes and meanwhile increase the hydrophilicity of the adhered active materials, and wettability of the electrodes.[12]

Even though there have been numerous studies regarding the paper-based electronics, there is not any available study on the wood-based electronics used natural wood slice directly as the flexible substrates. As the most abundant natural porous carbon material in the world, wood has an inartificial hierarchical cellular structure containing microscale structures of cut cell walls on transverse sections and excellent hydrophilic properties due to the hydroxyl group.[13] Here, we use wood sliced at a transverse section with a thickness of 100 μm as the flexible porous substrate. Wood may be cut in three ways: transverse section, radial section, and tangential section. Only the wood transverse section slice (WTSS) has a 3D honeycomb porous structure (Fig. S1†). It makes transverse section slice has a relatively high specific surface area than the other two sections sliced at the same thickness.[14] So, when the active materials are attached on the surface of the WTSS, the specific surface area of active materials layer is also increased. More importantly, wood instinctively absorbs sorts of ions and water in the metabolic process by means of its vessels and tracheids.[15] So, WTSS can effectively absorb the electrolytes by capillary action and can function as an electrolyte reservoir.[16] This characteristic provides the ions with additional and continuous transport pathways through the active material phase to the electrolyte phase, causing rapid kinetics of ion transport.

In this work, we use natural WTSS as the flexible porous substrate without any chemical treatment and polypyrrole (PPy) as the active material to create a flexible porous composite electrode. PPy is a conducting polymer with high conductivity, inherent fast redox switching, and is more environmental-friendly and cost-efficient than most metal containing active materials.[17] PPy can easily be integrated into WTSS with hydrogen bond, generating a strong adhesion.[18] When soaked into monomer liquid of PPy, WTSS absorbs the liquid into its porous structure with PPy's polymerization followed, then a porous flexible PPy-coated WTSS (abbreviated as WTSS/PPy) electrode material formed. This composite electrode material is highly conductive and can be used to assemble flexible solid-state supercapacitor. This method will be easily to proceed to get supercapacitor at low cost, and makes the WTSS/PPy sheet a unique alternative candidate for flexible energy storage device using wood resource.

Experimental

Preparation of PPy/WTSS electrode

Native WTSSs were produced from Chinese fir using KD 2258 rotary microtomy without any chemical treatment and the thickness was about 100μm. The wood slices were cut to 1.0× 2.0 cm^2 and subsequently vacuum dried at 40 °C for 3 h. A sample of 0.1 g/mL ferric chloride solution was prepared by adding 10g of ferric chloride into 100 mL 0.3 M hydrochloric

acid. Firstly, the wood slices were immersed in the pyrrole monomer for 3 minutes, then picked them out and drained off the liquid on the surface. After that, the slices were transferred into the ferric chloride solution to polymerize at 5°C for different times of 10, 30, 60, and 180 minutes. The slices were picked out and washed with 0.3 M hydrochloric acid and deionized water to remove any residue. Finally, the slices were dried vacuum at 40 °C for 3 h. The pyrrole monomer was purchased from Aladdin Industrial Corporation and the rest were purchased from Beijing Chemical Reagents Company of analytical grade.

Preparation of solid-state supercapacitors

Two WTSS/PPy electrodes were assembled into a flexible supercapacitor in a traditional two-electrode laminated configuration by sandwiching a PVA/H_3PO_4 gel as the electrolyte and simultaneous separator between the two electrodes. To be specific, two pieces of the WTSS/PPy electrode were soaked in PVA/H_3PO_4 solution for at least 30 min to make sure the wood pores had fully absorbed the electrolyte. Then, the electrodes were removed from the solution to evaporate excess water at room temperature. The two sections of the WTSS/PPy electrodes were pressed together tightly to form a gel-electrolyte layer between them. This method minimizes the supercapacitors thickness and simplifies the fabrication process.

Characterization

X-ray photoelectron spectroscopy (XPS) was carried out with a PHI 5300 Photoelectron Spectrometer (Perkin 15 Elmer Instruments Co. Ltd., USA). Scanning electron microscopy (SEM) and energy dispersive spectrometer (EDS) were performed using a Hitachi S-4800 field-emission-gun scanning electron microscope (Japan) at 5.0 kV. Fourier transform infrared spectra (FTIR) were recorded by Nicolet 6700 spectrometer (Thermo Electron Scientific Instruments Co. Ltd., USA). Dynamic mechanical analysis (DMA) tests were measured by Anton Paar Physica MCR 301. Conductivity was measured by a ST 2253 4-point probes resistivity measurement system (Suzhou Jingge Electronic Co., Ltd). The electrochemical measurements were evaluated using a two-electrode test cell on a CHI 660E electrochemical workstation (CH Instruments Inc.) at room temperature.

Results and discussion

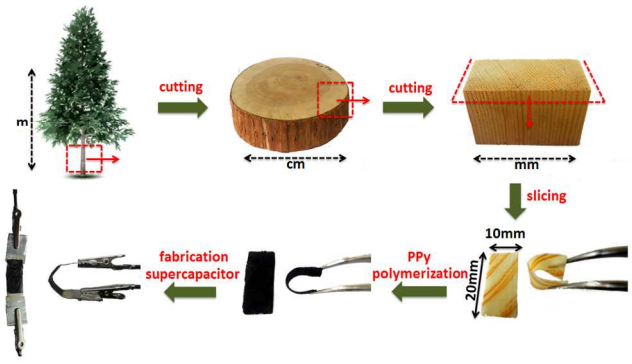

Fig. 1. Schematic diagrams of the preparation process of native WTSS, WTSS/PPy and its supercapacitor.

The preparation process of native WTSS, WTSS/PPy electrode and its supercapacitor is illustrated in Fig. 1. When the PPy polymerized onto the WTSS, WTSS texture colors turn into black gradually. WTSS is very flexible and can be bent to 180 degree very easily, which gives the WTSS/PPy electrode and its supercapacitor good flexibility, as showed in Fig. 1. We use Chinese fir as the substrate material of WTSS because its light and soft texture, which make it easy to cut a smooth slice. More importantly, as a softwood lumber, the tracheid of Chinese fir is arranged evenly and orderly. The nature Chinese fir has a specific surface area of 22.37 m^2/g and porosity of 80.50% measured with mercury intrusion porosimetry (MIP) in our previous study,[19] which endow a good utilization of PPy and favorable transportation corridors for electrolyte.

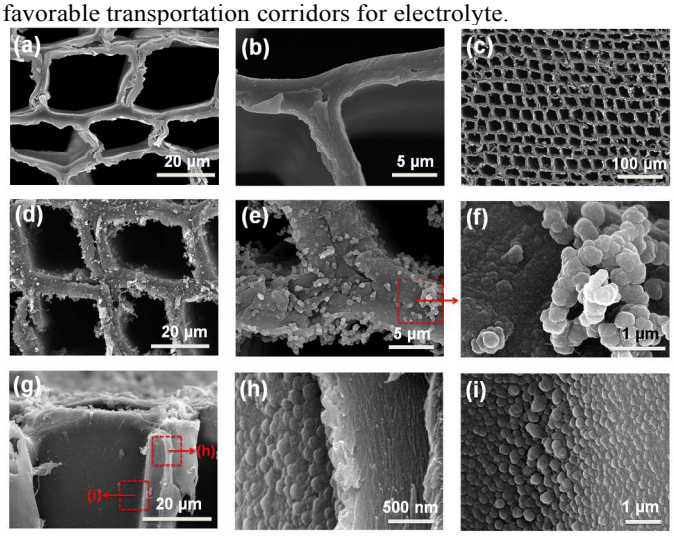

Fig. 2. SEM images of (a) and (b) WTSS at different scales. SEM images of (c), (d) and (e) the 180 minutes WTSS/PPy at different scales. (f) is detail with enlarged scale of red marker in image (e). (g) Cross-section SEM images of the 180 minutes WTSS/PPy. (h) and (i) are details with enlarged scale of red marker in image (g).

Morphological characteristics before and after the PPy was polymerized on the WTSS were examined with scanning electron microscopy (SEM). Fig. 2a to 2i shows the surface morphology of the bare WTSS and WTSS/PPy at different degrees of magnification. The 3D honeycomb porous structure of the tracheid cell wall can be clearly identified (Fig. 2a). Both the section and inner wall surface of tracheid cell wall are very smooth (Fig. 2b). However, when PPy is polymerized on WTSS, the coarse particulate matters can be observed in the porous structure (Fig. 2d). The surface of tracheid cell wall is no longer smooth, and a PPy layer is clearly observed adhering to the cell wall (Fig. 2e). Some PPy agglomerates were formed and dispersed throughout the structure in the more magnified image (Fig. 2f) of the red-squared marker region in Fig. 2e. Although the modification makes the WTSS surface rough, the porous structure of the WTSS still maintains integrity (Fig. 2c). The porous structure of the WTSS is not clogged by PPy, which ensures the functionality of electrolyte reservoir. A cross section of WTSS/PPy is shown in Fig. 2g. There is no obvious particulate matter observed in the inner wall surface of the tracheid cell wall at the similar magnification as Fig. 2d. However, in the corresponding high magnification image (Fig. 2h, 2i) of the red-squared marker region, the dense bulged small PPy particles with size around 200-500 nm are visible. This means that all the inner wall surface of the tracheid cell walls are successfully coated by the PPy layer, which endows

WTSS/PPy a high electrical conductivity of 1.92 S cm^{-1}. A clear interface between the wood and the PPy cross-section can be seen from the SEM image in Fig. 2h and the PPy layer thickness is around 100 nm. Due to the 3D honeycomb porous structure of the WTSS/PPy (pore size about 20-30μm, as showed in Fig. 2d), WTSS/PPy can absorb electrolyte solution very well. So, this porous structure is an ideal reservoir and channel for electrolyte absorption. Meanwhile, the porous characteristic and granular morphology cause a relatively high specific surface area for WTSS/PPy, which increases the contact area between electrolyte and PPy. Overall, all these properties provide a good utilize efficiency of the active material and favorable transportation corridors for electrolyte, and thus they promote the electrochemical performance.

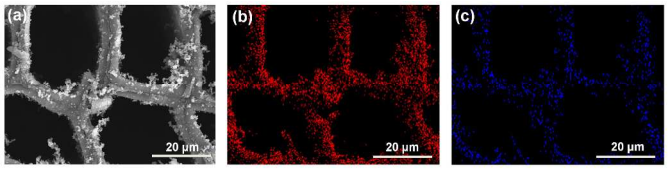

Fig. 3. (a, b and c) SEM/EDS image of the 180 minutes WTSS/PPy. (b and c) Corresponding elemental mapping images of (b) N, and (c) Cl.

Furthermore, energy dispersive spectrometer (EDS) test of the 180 minutes WTSS/PPy provides a clearly elemental distribution of the PPy (Fig. 3a-c). The elemental mapping (Fig. 3b, c) revealed that the nitrogen chlorine atoms were doped into the WTSS/PPy. Meanwhile, the nitrogen and chlorine atoms were uniformly distributed throughout the 3D honeycomb porous structure of the WTSS, demonstrating that the PPy were successfully polymerized onto the WTSS substrate.

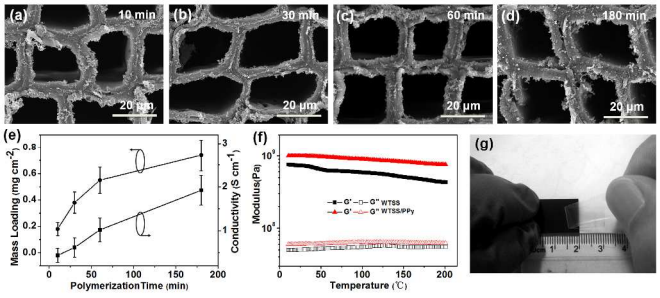

Fig. 4. (a–d) SEM images for WTSS/PPy with different polymerization times of 10, 30, 60 and 180 minutes, respectively. (e) Mass loadings of polypyrrole and conductivity of WTSS/PPy with respect to polymerization times of 10, 30, 60 and 180 minutes. (f) Dynamic mechanical behavior of WTSS and the 180 minutes WTSS/PPy. (g) WTSS/PPy passes the tape test shows that the strong mechanical property.

Generally speaking, longer polymerization time could give rise to incremental mass loadings of the PPy and microtopography change of the WTSS/PPy. However, no apparent microtopography change can be observed with increased polymerization time (Fig. 4a-d). The porous nature of WTSS remains even after PPy coating. The mass loading of PPy polymerized onto WTSS is about 0.18, 0.38, 0.55 and 0.74 mg cm^{-2} with a polymerization time of 10, 30, 60, and 180 minutes, respectively (Fig. 4e). Correspondingly, the conductivity of WTSS/PPy is 0.44, 0.62, 1.02 and 1.92 S cm^{-1} with polymerization time ranging from 10 to 180 minutes, respectively (Fig. 4e). This high conductivity assures that the WTSS/PPy electrode can be used as a flexible current collector. In order to achieve the maximum capacitance per geometric area, in this study we focused on the 180 minutes WTSS/PPy. WTSS/PPy with polymerization times of 10, 30 and 60 minutes were used for comparison purposes.

The mechanical behavior of the WTSS and the 180 minutes WTSS/PPy was examined using dynamic mechanical analysis tests (Fig. 4f). The storage moduli (*G'*) of WTSS and WTSS/PPy decrease slowly as temperature increases, and are much larger than the corresponding loss moduli (*G''*), and all their *G* values are greater than 10^7 Pa, indicating that these materials have strong mechanical properties. The *G'* of WTSS/PPy is higher than that of WTSS alone, which shows that PPy can enhance the strength of WTSS.

In order to confirm the strong adhesion between the PPy and WTSS substrate, the mechanical adhesion is also tested by tape. No obvious PPy could be observed on tape, further showing good adhesion of the PPy on the WTSS substrate (Fig. 4d). In fact, the mechanical adhesion between the PPy and WTSS is quite strong because of the hydrogen bond interaction between the N of pyrrole rings and the hydroxyl groups of cellulose in wood.[18] Further, this strong mechanical adhesion ensures mechanical stability of flexible WTSS/PPy electrode and its supercapacitor in the bending process.

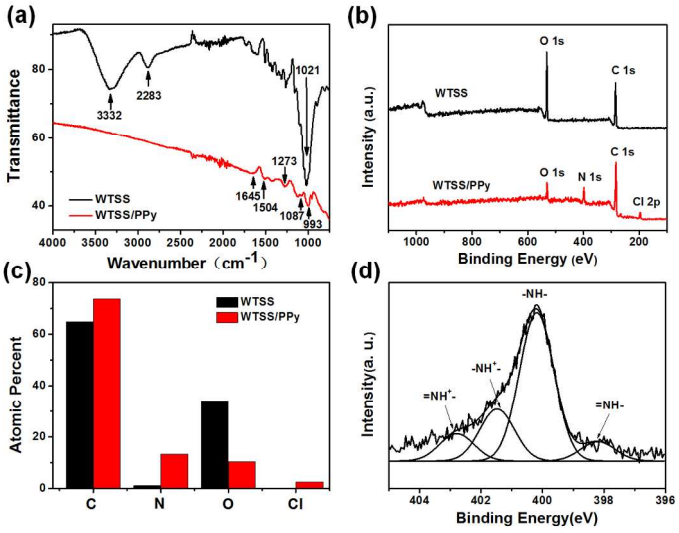

Fig. 5. (a) FTIR spectra of WTSS and the 180 minutes WTSS/PPy. (b) XPS spectra of WTSS and the 180 minutes WTSS/PPy. (c) Atomic percent values for WTSS and the 180 minutes WTSS/PPy from XPS test. (d) N 1s XPS spectrum on the 180 minutes WTSS/PPy.

Fourier transform infrared spectroscopy (FTIR) of both the bare WTSS and the 180 minutes WTSS/PPy were measured to study the chemical compositions change (Fig. 5a). A broad band around 3332 cm^{-1} is the stretching vibration of -OH group in cellulose. The bands at 2283 cm^{-1} and 1021 cm^{-1} belong to the asymmetrically stretching vibration of $-CH/-CH_2$ and $-CO$ respectively.[20] However, after PPy polymerized on WTSS, the FTIR spectrum is almost the characteristic signals of PPy, which indicates that the WTSS surface was completely covered with PPy. The peaks around 1645, 1087 and 993 cm^{-1} denote the absorption of C=C in-ring-stretching, C–C in-ring-stretching, and C–H out-of-plane deformation vibration,

respectively.[21] In addition, the weak bands that appear at 1504 cm^{-1} and 1273 cm^{-1} are assigned to the C–N stretching vibration of PPy.[22] The surface chemical elements of WTSS before and after PPy coated were further characterized by X-ray photoelectron spectroscopy (XPS) and the result was displayed in Fig. 5b. The full scan spectra of bare WTSS show only two obvious peaks of oxygen and carbon. Percentage contents of carbon and oxygen calculated from the XPS are about 64.8% and 35.1% (Fig. 5c). These chemical elements are mainly contributed by the cellulose, lignin and hemicellulose in wood. As for WTSS/PPy, there are four chemical elements in the full scan spectra, which are oxygen, nitrogen, carbon and chlorine with percentage content of 10.41%, 13.36%, 73.65% and 2.57%, respectively (Fig. 5c). The nitrogen almost entirely comes from the PPy, and the chlorine elements demonstrate that PPy is doped with ferric chloride during the chemical polymerization. Moreover, the XPS spectrum of N 1s in WTSS/PPy was deconvoluted into separate peaks in order to interpret the electrical properties of the PPy (Fig. 5d). The four component peaks are –NH= at 398.2eV, –NH– at 400.2eV, $–NH^{+}–$ at 401.5eV and $–NH^{+}=$ at 402.8eV.[23] Thus, the FTIR and XPS results indicate that the active material doped PPy is successfully introduced onto the surface of the porous structured WTSS.

The electrochemical performance of the 180 minutes WTSS/PPy electrode fabricated flexible supercapacitor cell was tested using a two-electrode test cell. For comparison, the WTSS/PPy electrode with the polymerization times 10, 30, 60 and 180 minutes based all-solid-state flexible supercapacitor was also evaluated (Fig. S2†). The results demonstrate that the 180 minutes WTSS/PPy electrode fabricated supercapacitor showed the biggest enclosed area on the CV curve at a fixed scan rate of 5 mV s^{-1} (Fig. S2a†), the longest charge–discharge time at a current density of 0.14 mA cm^{-2} (Fig. S2b†) and a lower ESR (Fig. S2c†) than the others. Hence, the energy storage capacity is also the largest among the four (Fig. S2d†), which can be attributed to its having the largest PPy loading amount.

The detailed electrochemical performance of the 180 minutes WTSS/PPy electrode fabricated supercapacitor is shown in Fig. 6. Fig. 6a shows the CV curves with sweep rates from 5 to 200 mV s^{-1}. The CV scan exhibits a rough rectangular mirror image without obvious redox peaks. With the increase of sweep rates, the CV curve remains rectangular with little distortion even at a high value of 200 mV s^{-1}. The results indicate that WTSS/PPy electrode has good rate capability and stability. These good performances should benefit from the excellent microscopic porous structure and hydrophilic properties of the WTSS substrate.[9]

Galvanostatic charge-discharge (GCD) studies of the 180 minutes WTSS/PPy electrode fabricated flexible supercapacitor cell were performed with cutoff voltage of 0–0.8 V at different discharge current densities, as shown in Fig. 6b. The charge and discharge curves show a nearly triangle, indicating good capacitive behaviors. The curves are not very straight mainly because of the pseudocapacitive behavior of PPy. Additionally, the internal resistance (IR) drop during the initial discharge is relatively small, illuminating that the supercapacitor cell has a low series resistance value. It is attributable to the good conductivity and porous characteristic of the WTSS/PPy electrode. With the increase of current density, the charge and discharge time become shorter. Because, the greater current density, the faster charge transfer rate in the inner electrolyte and electrode, and the shorter reach time required for the upper and lower limit of the charging voltage.

The electrochemical performance of the supercapacitor cell was further examined by EIS analysis, as shown in Fig. 6c. In the high-frequency region (Fig. 6c inset), the equivalent series resistance (ESR) in the real axis intercept is relatively small, showing the good conductivity of the WTSS/PPy electrode. It agrees with the results of GCD curves. At the medium frequency region, the straight line with an angle of about 45° represents the relatively lower Warburg resistance of the electrolyte ions diffusion.[24,25] It may be because the 3D honeycomb porous structure of the WTSS/PPy electrode promotes the transmission efficiency of electrolyte ions.

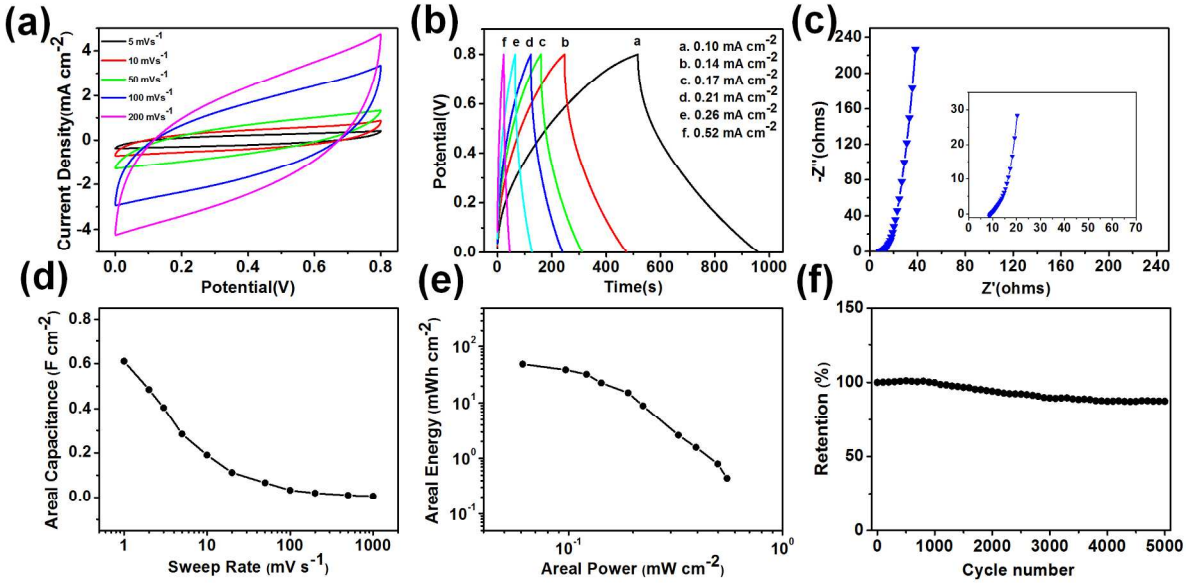

Fig. 6. CV (a), GCD (b) and EIS (c) curves of the 180 minutes WTSS/PPy fabricated supercapacitor, respectively. The inset of (c) shows an enlarged scale at high frequency. (d) Areal capacitance of the 180 minutes WTSS/PPy electrode at different sweep rates. (e) Areal power against areal energy plot of the 180 minutes WTSS/PPy fabricated supercapacitor. (f) Cyclic stability of the 180 minutes WTSS/PPy fabricated supercapacitor measured at a sweep rate of 50 mV s^{-1}.

The areal capacitance was calculated using CV curves at different sweep rates to assess the charge storage capacitance of the flexible supercapacitor cell, as shown in Fig. 6d. The 180 minutes WTSS/PPy electrode demonstrates high areal capacitance of about 0.61 F cm^{-2} at a low sweep rate of 1 mV s^{-1}. The gravimetric capacitance calculated from the discharge curves has about 408 F g^{-1} at a current density of 0.10 mA cm^{-2} (Fig. S2d†). Even at a high current density of 0.21 mV s^{-1}, the capacitance still remains a value of 213 F g^{-1} (52% of the initial capacitance). With the increase of sweep rate, the WTSS/PPy electrode shows a good rate capability. The areal capacitance here is much higher than that of other flexible electrodes values that have been reported recently,[26,27] which is reasonable due to the 3D honeycomb porous structure of the WTSS/PPy electrode. This structure improves the accessible surface area of the active material and effectively facilitates electrolyte ion diffusion.

A ragone plot of areal specific power against areal specific energy for the supercapacitor cell is shown in Fig. 6e. It can be observed that the areal specific power decreases gradually with the increasing of areal specific energy of the cell. The plot shows the maximum areal energy of 48.83 mWh cm^{-2} and areal power of 0.55 mW cm^{-2}. The areal specific energy and specific power density result are superior to the previously reported for paper substrates.[26,27] The good areal specific energy and specific power density value may be results of the higher ion accessibility in the 3D honeycomb porous structure of the WTSS/PPy electrode.

The cyclic stability of the 180 minutes WTSS/PPy fabricated flexible supercapacitor cell was evaluated using CV with a sweep rate of 50 mV s^{-1}, as shown in Fig. 6f. The capacitance increases slightly in the first 1000 cycles, then decreases quickly in the middle 3000 cycles and finally decreases slowly in the following cycles. After 5000 times of cycling, the capacitance still retained 87.5% of the initial capacitance, demonstrating a good cycling stability of flexible supercapacitor cell. The cycling performance of the WTSS/PPy fabricated flexible supercapacitor is much better than some reported results for PPy-based supercapacitors.[28]

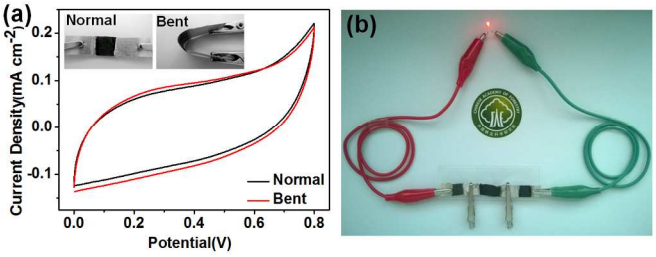

Fig. 7. (a) Comparison of CV curves at 1 mV s^{-1} for the 180 minutes WTSS/PPy fabricated supercapacitor cell tested under normal and bent state. (b) Digital picture of a red LED lit by an in-series fabricated supercapacitor cell with three units.

For further understanding the flexibility performances, the capacitive performances at normal and bent states were evaluated by CV measurements at a sweep rate of 1 mV s^{-1}. As seen in Fig. 7a, the bent state had almost no effect on the capacitive behavior of 180 minutes the WTSS/PPy fabricated flexible supercapacitor, and the flexible WTSS/PPy electrode at bent state even had a higher areal capacitance of about 0.63 F cm^{-2}. These results show the WTSS/PPy fabricated supercapacitor has good flexibility, which can be exploited to meet various commercial applications. This flexibility can be attributed to the fact that wood is a remarkable natural composite material with admirable native mechanical performance, that plays a strong role as a skeleton for active materials. Additionally, it was demonstrated that a red light-emitting diode (LED) was able to be lit by the in-series fabricated supercapacitor cell with three units (Figure 7b).

Conclusions

An interesting device is reported to construct mechanically flexible wood-based all-solid-state supercapacitor by assembling polypyrrole (PPy) coated wood transverse section slice (WTSS) composite electrodes for the first time. Owing to the 3D honeycomb porous structure and hydrophilicity characteristics of the WTSS substrate, PPy-coated WTSS electrode has good specific capacitance, areal power and excellent cyclic stability. These better electrochemical performances can be attributed to the extra ion diffusion pathway realized through the electrolyte uptake by the WTSS. The novel electrode has an areal capacitance of 0.61 F cm^{-2} or 408 F g^{-1} (based on the mass of PPy) at a low sweep rate of 1 mV s^{-1} and retains 87.5% capacitance after 5000 cycles. This fabricated supercapacitor cell exhibits good mechanical flexibility and has a high energy density of 48.83 mWh cm^{-2} and power density of 0.55 mW cm^{-2}. Perhaps natural wood is not the most suitable substrate material, but we try to give a new candidate for future flexible energy storage device.

Acknowledgements

This work was supported by the National Natural Science Foundation of China (NO.31400504), and the Special Fund of Chinese Central Government for Basic Scientific Research Operations in Commonweal Research Institutes (NO.CAFINT2014K02).

Notes and references

[a] Research Institute of Wood Industry, Chinese Academy of Forestry, Beijing 100091, China. E-mail:lvsy@caf.ac.cn.
[b] Center for Renewable Carbon, University of Tennessee, Knoxville, Tennessee, 37996, USA

†Electronic Supplementary Information (ESI) available: Electrochemical characterization in details, and some electrochemical properties. See DOI: 10.1039/c000000x/

1 Y. Qi and M. C. McAlpine, *Energy Environ. Sci.*, 2010, **3**, 1275-1285.
2 S. Liu, T. Yu, Y. Wu, W. Li and B. Li, *RSC Adv.*, 2014, **4**, 34134-34143.
3 L. Li, Z. Wu, S. Yuan and X.-B. Zhang, *Energy Environ. Sci.*, 2014, **7**, 2101-2122.
4. K. Gao, Z. Shao, X. Wu, X. Wang, Y. Zhang, W. Wang and F. Wang, *Nanoscale*, 2013, **5**, 5307-5311.
5. D. Tobjörk and R. Österbacka, *Adv. Mater.*, 2011, **23**, 1935-1961.
6. G. Zheng, L. Hu, H. Wu, X. Xie and Y. Cui, *Energy Environ. Sci.*, 2011, **4**, 3368-3373.
7. L. Hu, M. Pasta, F. L. Mantia, L. Cui, S. Jeong, H. D. Deshazer, J. W. Choi, S. M. Han and Y. Cui, *Nano Lett.*, 2010, **10**, 708-714.
8. K. Jost, C. R. Perez, J. K. McDonough, V. Presser, M. Heon, G. Dion and Y. Gogotsi, *Energy Environ. Sci.*, 2011, **4**, 5060-5067.

9. A. Vu, Y. Qian and A. Stein, *Adv. Energy Mater.*, 2012, **2**, 1056-1085.
10. K. Gao, Z. Shao, X. Wang, Y. Zhang, W. Wang and F. Wang, *RSC Adv.*, 2013, **3**, 15058-15064.
11. Y. Li, Z. Y. Fu and B. L. Su, *Adv. Funct. Mater.*, 2012, **22**, 4634-4667.
12. G. Zheng, Y. Cui, E. Karabulut, L. Wågberg, H. Zhu and L. Hu, *MRS Bull.*, 2013, **38**, 320-325.
13. S. Trey, S. Jafarzadeh and M. Johansson, *ACS Appl. Mater. Interfaces*, 2012, **4**, 1760-1769.
14. J.L. Bowyer, R.Shmulsky, J.G. Haygreen, *Forest products and wood science: an introduction*, *5th ed*, Wiley-Blackwell, New Jersey, 2007.
15. D.N.S. Hon, N. Shiraishi, *Wood and cellulosic chemistry, 2nd ed*, CRC Press, Boca Raton, 2000.
16. H. Zhu, Z. Jia, Y. Chen, N. Weadock, J. Wan, O. Vaaland, X. Han, T. Li and L. Hu, *Nano Lett.*, 2013, **13**, 3093-3100.
17. P. Novák, K. Müller, K. Santhanam and O. Haas, *Chem. Rev.*, 1997, **97**, 207-282.
18. C. Sasso, D. Beneventi, E. Zeno, D. Chaussy, M. Petit-Conil and N. Belgacem, *BioResources*, 2011, **6**, 3585-3620.
19. S. He, L. Lin, F. Fu, Y. Zhou and M. Fan, *BioResources*, 2014, **9**, 1924-1938.
20. Z.-l. Mo, Z.-l. Zhao, H. Chen, G.-p. Niu and H.-f. Shi, *Carbohydr. Polym.*, 2009, **75**, 660-664.
21. X.-G. Li, A. Li, M.-R. Huang, Y. Liao and Y.-G. Lu, *J. Phys. Chem. C*, 2010, **114**, 19244-19255.
22. L. Qu, G. Shi, F. e. Chen and J. Zhang, *Macromolecules*, 2003, **36**, 1063-1067.
23. K. Jradi, B. Bideau, B. Chabot and C. Daneault, *J. Mater. Sci.*, 2012, **47**, 3752-3762.
24. Y. J. Kim, I. Y. Jang, K. C. Park, Y. C. Jung, T. Oka, S. Iinou, Y. Komori, T. Kozutsumi, T. Hashiba and Y. A. Kim, *Electrochim. Acta*, 2010, **55**, 5624-5628.
25. G. Pandey, S. Hashmi and Y. Kumar, *J. Electrochem. Soc.*, 2010, **157**, A105-A114.
26. X. Wang, A. Sumboja, W. L. Foo, C. Y. Yan, K. Tsukagoshi and P. S. Lee, *RSC Adv.*, 2013, **3**, 15827-15833.
27. Z. Weng, Y. Su, D. W. Wang, F. Li, J. Du and H. M. Cheng, *Adv. Energy Mater.*, 2011, **1**, 917-922.
28. L. Yuan, B. Yao, B. Hu, K. Huo, W. Chen and J. Zhou, *Energy Environ. Sci.*, 2013, **6**, 470-476.

